JOURNAL OF COMPUTATIONAL PHYSICS 94, 59–80 (1991)

A Comparison of Different Propagation Schemes for the Time Dependent Schrödinger Equation

C. LEFORESTIER,[1] R. H. BISSELING,[2] C. CERJAN,[3] M. D. FEIT,[3] R. FRIESNER,[4] A. GULDBERG,[5] A. HAMMERICH,[6] G. JOLICARD,[7] W. KARRLEIN,[8] H.-D. MEYER,[9] N. LIPKIN,[10] O. RONCERO,[1] AND R. KOSLOFF[6]

CECAM Workshop, Université de Paris-Sud, 91405 Orsay, France

Received September 29, 1989; revised January 10, 1990

A comparison of three widely used time propagation algorithms for the time dependent Schrödinger equation is described. A typical evolution problem is chosen to demonstrate the efficiency and accuracy of the various methods on a numerical grid using a pseudo-spectral (FFT) spatial representation for scattering and bound state evolution. The methods used —second-order differencing, split operator propagation, Chebyshev polynomial expansion—are discussed in terms of their applicability to various classes of dynamic problems. A new method is introduced which is based upon a low-order Lanczos technique. This method appears to offer an accurate and flexible alternative to the existing techniques. Overall the Chebyshev method is recommended for time independent potentials and the Lanczos method for time dependent potentials.

I. INTRODUCTION

Quantum mechanical treatment of molecular processes constitutes an important part in the understanding of basic atomic and molecular phenomena. Modeling these systems based on first principles is a source of insight into fundamental dynamical behavior. The ability to successfully simulate a molecular process is the final proof that the phenomena is well understood. Among the methods for quan-

[1] Laboratoire de Chimie Théorique, Université de Paris-Sud, 91405 Orsay, France.
[2] Koninklijke/Shell-Laboratorium, Amsterdam, P.O. Box 3003, 1003 AA Amsterdam, The Netherlands.
[3] Lawrence Livermore National Laboratory, Livermore, CA 94550.
[4] Department of Chemistry, University of Texas, Austin, TX 78712.
[5] Institute for Chemistry, Radmansquade 71, 2200 N Copenhagen, Denmark.
[6] Department of Physical Chemistry and The Fritz Haber Research Center for Molecular Dynamics, The Hebrew University, Jerusalem 91904, Israel.
[7] Laboratoire de Physique Moléculaire, Université de Besançon, 25030 Besançon, France.
[8] Institut für Physikalische Chemie, Marcusstr. 9–11, 8700 Würzburg, Germany.
[9] Physikalisch-Chemisches Institut, Universität Heidelberg, Im Neuenheimer Feld 253, D-6900 Heidelberg, Germany.
[10] Department of Chemistry, Technion-Israel Institute of Technology, 32000 Haifa, Israel.

0021-9991/91 $3.00

tum mechanical calculations, time dependent methods have emerged as an important technique for researchers in this field. The success of these methods can be attributed to their natural correspondence to experiment—starting from an initial state and following the events through time—naturally generalizing the intuitive classical description. Moreover, recent progress in time dependent methods, in particular the introduction of grid representations, has made the method competitive with other exact quantum mechanical calculations.

A numerical solution of the time dependent Schrödinger equation basically consists of two part. The first part is a faithful discrete spatial representation of the wavefunction $\psi(x, t)$. Once such a representation is constructed an initial wavefunction can be propagated in time. It is this second propagation stage that is the subject of this paper.

The scope of this paper is limited to methods for which the error can be controlled, i.e., the error can be reduced indefinitely. This paper is motivated by grid methods but the formulation can be extended to other representations. The use of grid methods to solve the time dependent Schrödinger equation can be traced back to the work of McCullough and Wyatt [1]. These authors used a finite difference scheme to calculate the kinetic energy term and a Crank–Nicholson (CN) propagation scheme borrowed from a numerical solver for a dissipative parabolic differential equation—the heat transport equation. Later it was shown by Askar and Cakmak that a second-order differencing propagation scheme has the same order accuracy as the CN method with much less numerical effort [2]. A similar scheme has been used by Leforestier for collision induced dissociation problems [3]. The replacement of the finite difference method for calculating the kinetic energy by the Fourier method has enhanced the accuracy of the spatial representation, since it possesses exponential convergence characteristics in contrast to the power law convergent finite differencing. This method has been developed by Feit *et al.* [4] using an operator propagation scheme adapted from an approach which they originally used for the paraxial equation [5]. An alternative Fourier method using a second-order differencing propagation scheme was developed by Kosloff and Kosloff [6] adapting a method which was used for the acoustical (Helmholtz) wave equation [7].

The fast proliferation and wide use of these methods [8] was the driving force behind the organization of the CECAM workshop in Orsay in October 1988. One of the issues considered was the properties of different propagation schemes used to solve the time dependent Schrödinger equation. The purpose of this paper, which was initiated in the CECAM workshop, is to compare the most common propagation schemes and to introduce a new propagation method. The issues to be considered are accuracy, numerical efficiency, and stability. It is hoped that this work can clarify the differences among the varying methods and facilitate the appropriate choice of propagation method suited for a particular problem. The four methods to be considered in this work are the second-order differencing scheme (SOD), the split operator scheme (SPO), the short iterative Lanczos propagator (SIL) and the Chebyshev scheme (CH). The methods are not always inter-

changeable but for the purpose of this comparison, a problem has been chosen in which all four methods are applicable.

The time dependent non-relativistic Schrödinger equation

$$i\hbar \frac{\partial \psi(t)}{\partial t} = \hat{\mathbf{H}}\psi(t) \tag{1.1}$$

where

$$\hat{\mathbf{H}} = \frac{\hat{\mathbf{P}}^2}{2m} + \hat{\mathbf{V}} \tag{1.2}$$

is the subject of this investigation. In order to compare the different propagation methods, a common spatial representation is used for the description of the wavefunction ψ and the Hamiltonian operation $\hat{\mathbf{H}}\psi$. The method chosen is the Fourier method in which the wavefunction ψ is represented on an equally spaced grid of sampling points in coordinate space. The potential operation $\hat{\mathbf{V}}\psi$ is local in this representation and is represented as $V_i\psi_i$ for each sampling point i. The same is true for any function of the potential, $f(\hat{\mathbf{V}})$, which becomes $f(V_i)\,\psi_i$ (pointwise multiplication). For example, in the split operator scheme the exponentiation $e^{-(i/\hbar)\hat{\mathbf{V}}t}\psi$ is required. The main point in the Fourier method is that the kinetic energy operation $(\hat{\mathbf{P}}^2/2m)\,\psi$ is also calculated locally. The transformation from the discrete coordinate representation to the discrete momentum representation and back is done via the fast Fourier transform (FFT) algorithm [9]. It has been shown that the representation of a typical wavefunction has exponential convergence properties with respect to grid size and density [10]. The algorithm scales with the number of grid points as $O(N \log N)$ compared to $O(N^2)$ matrix operations for a straightforward discretization method. (It should be noted that in practice, all N^2 operations are not required—the order enters as the bandedness of the discretization method). From a computational point of view the FFT algorithm is the most time consuming part of the Hamiltonian operation. Maximizing numerical efficiency means minimizing the number of FFT calls per propagation step which might include many substeps.

The spatial representation has an important influence on the time propagation. The discrete representation of the Hamiltonian operation restricts the energy range of the problem. This energy range imposes an upper bound to the high frequency components represented in the propagation, $\omega_g = \Delta E_{\text{grid}}/\hbar$. This bound on the frequency is common to all methods and therefore can serve as a reference to test numerical efficiency. In the discrete Fourier representation, the range of eigenvalues for the Hamiltonian operator, $\Delta E_{\text{grid}} = E_{\max} - E_{\min}$, is estimated by adding the upper and lower bounds of the kinetic and potential energy represented on the grid

$$E_{\max} = V_{\max} + K_{\max} \tag{1.3}$$

and

$$E_{\min} = V_{\min}, \tag{1.4}$$

with

$$K_{\max} = \sum_i \frac{\pi^2 \hbar^2}{2m_i (\Delta q_i)^2}, \tag{1.5}$$

where m_i and Δq_i are the mass and grid spacing of the ith coordinate.

The common use of the same representation technique for all propagation methods places each scheme on an equal footing. Nevertheless, for a particular application one should balance the error in the spatial representation with the error in the propagation scheme.

II. Time Propagation

The time dependent Schrödinger equation (1.1) has the formal solution

$$\psi(t) = \mathbf{U}(t)\,\psi(0) = \hat{\mathbf{T}} \exp\left(-\frac{i}{\hbar} \int_0^t \hat{\mathbf{H}}(t')\,dt' \right) \psi(0), \tag{2.1}$$

where $\hat{\mathbf{T}}$ is the time ordering operator. A simple solution to the time problem is to break up the total evolution operator into small increments of duration Δt in which the variation of the Hamiltonian operator is small

$$\hat{\mathbf{U}}(t) = \prod_{n=0}^{N-1} \hat{\mathbf{U}}((n+1)\,\Delta t, n\,\Delta t), \tag{2.2}$$

where $\Delta t = t/N$ and

$$\hat{\mathbf{U}}(t + \Delta t, t) = e^{-(i/\hbar)\hat{\mathbf{H}}(t)\Delta t}. \tag{2.3}$$

In the example used in this paper a time independent Hamiltonian is assumed. Therefore there is no restriction on the size of Δt (time-ordering is irrelevant). The differences between the propagation schemes can be traced to the way the exponentiation in Eq. (2.3) is approximated.

III. Spectral Efficiency

The next task is to set guidelines for comparison of the accuracy of the methods considered. Rather than calculate the absolute accuracy in any particular situation it is more important to obtain a measure of the accuracy with the numerical effort required. This viewpoint links the accuracy with the numerical effort needed to

achieve it. The problem is somewhat complicated because in most propagation methods errors accumulate, therefore one should find the scaling of the accuracy with the propagation time. These scaling laws can be used as guidelines for choosing the appropriate propagation scheme.

As was mentioned above the numerical efficiency can be measured in relation to typical frequencies in the problem. One such frequency is the maximum frequency ω_g imposed by the discretization scheme. Another natural frequency is determined by the energy spread of the wavefunction $\Delta E_{\text{wave}} < \Delta E_{\text{grid}}$ which is the energy range that contains an overwhelming percentage of the wavefunction $\omega_w = \Delta E_{\text{wave}}/\hbar$. This idea comes from the practical observation that in most time dependent calculations the energy spectrum of the wavefunction is concentrated in a band and is not equally distributed. The typical choice is a wavepacket which has a Gaussian distribution of momentum and coordinate observables. The energy of this wavefunction is distributed as

$$p(E) = \exp\left(-\frac{m(\sqrt{E}-\sqrt{E_0})^2}{\sigma_p^2}\right). \tag{3.1}$$

In this case ΔE_{wave} is defined by the variance of the momentum σ_p, the mass m, and a tolerance chosen by the probability to be out of the energy band. For other common wavefunctions such an energy band is quite typical, or sometimes several energy bands dominate the energy spectrum.

An important issue for an efficient calculation is the balance between wavefunction frequency ω_w with the frequency supported by the grid ω_g. The ratio

$$\eta_g = \frac{\omega_w}{\omega_g}, \tag{3.2}$$

measures the static efficiency of the wavefunction with respect to the grid: a measure of the occupied to available phase space on the grid.

A dynamic frequency which is the actual frequency used by the propagation scheme can be defined as

$$\omega_D = \frac{N}{\Delta t}, \tag{3.3}$$

where N is the number of times the Hamiltonian operation is called per time step. (For a fixed global time step this is a constant.) The dynamical efficiency of the propagation can be defined as the ratio of the frequencies ω_g and ω_w to the static dynamical frequency

$$\eta_{Dg} = \frac{\omega_g}{\omega_D} \tag{3.4}$$

and

$$\eta_{Dw} = \frac{\omega_w}{\omega_D}. \tag{3.5}$$

The efficiency measures in Eqs. (3.2), (3.4), and (3.5) will aid in the comparison among the different propagation schemes.

It should be mentioned that a total shift in the energy scale which has no measurable consequences (that is, a constant phase shift multiplying the wavefunction) can have a significant influence on approximate propagation schemes. This property is used for efficient propagation of the SOD and CH schemes.

The different propagation schemes can also be compared with respect to a list of properties which have an important bearing on their applicability. The first of these properties is stability. Propagation schemes might not be stable to repeated use which is required in Eq. (2.2). The numerical manifestation of this instability is an exponential overflow. First-order differencing schemes are examples of methods which can be divided into unconditionally stable methods—for which there is no limit to the size of the time step—and methods which are conditionally stable—the time step is required to be less than some Δt_{stable}. Stability is not directly connected to accuracy and a stable method can produce inaccurate results. Usually unconditionally stable methods are also unitary in the sense that the normalization of the wavefunction is preserved. Another issue is that the applicability of the method be clear, since not all spatial representations of the Hamiltonian operation can be used by all methods. In the sections to follow a description of four propagation schemes is presented.

IV. Global Propagator: The Chebyshev Scheme (CH)

Global propagators can be defined by their use of very long time steps, sometimes a single time step completes the calculation. The main idea behind global propagators is to use a polynomial expansion of the exponential in the evolution operator

$$\hat{\mathbf{U}}(t) = e^{-(i/\hbar)\hat{\mathbf{H}}t} \approx \sum_{n=0}^{N} a_n P_n\left(-\frac{i}{\hbar}\hat{\mathbf{H}}t\right). \tag{4.1}$$

The problem then becomes the choice of the optimal polynomial approximation.

The Chebyshev scheme [11] approaches this problem in analogy to the approximation of a scalar function. Consider a scalar function $F(x)$ in the interval $[-1, 1]$. In this case it is known that the Chebyshev polynomial approximations are optimal, since the maximum error in the approximation is minimal compared to almost all possible polynomial approximations.

In the approximation of the evolution operator, the complex Chebyshev polynomials $\Phi_n(\hat{\mathbf{X}})$ are used, replacing the scalar function by a function of an operator. In making this change, one has to examine the domain of the operator and adjust it to the range of definition of the Chebyshev polynomials. The range of definition of these polynomials is from $-i$ to i. This means that the Hamiltonian operator has to be renormalized by dividing by $\Delta E_{\text{grid}} = E_{\max} - E_{\min}$. Also, for maximum

efficiency, the range of eigenvalues is positioned from -1 to 1 by shifting the Hamiltonian to

$$\hat{\mathbf{H}}_{\text{norm}} = 2\,\frac{\hat{\mathbf{H}} - \hat{\mathbf{I}}(\Delta E_{\text{grid}}/2 + E_{\text{min}})}{\Delta E_{\text{grid}}}. \tag{4.2}$$

With this definition, the evolution of the wavefunction ψ can be approximated as

$$\psi(t) \approx e^{-(i/\hbar)(\Delta E_{\text{grid}}/2 + E_{\text{min}})t} \sum_{n=0}^{N} a_n\left(\frac{\Delta E_{\text{grid}} \cdot t}{2\hbar}\right) \Phi_n\{-i\hat{\mathbf{H}}_{\text{norm}}\}\,\psi(0), \tag{4.3}$$

where the Φ_n are the complex Chebyshev polynomials. The first term on the right-hand side is a phase shift compensating the shift in the energy scale. The expansion coefficients becomes

$$a_n(\alpha) = \int_{-i}^{i} \frac{e^{i\alpha x}\Phi_n(x)\,dx}{(1-x^2)^{1/2}} = 2J_n(\alpha) \tag{4.4}$$

with $a_0(\alpha) = J_0(\alpha)$ and $\alpha = \Delta E_{\text{grid}} \cdot t/2\hbar$. Considering the propagation algorithm, the use of Eq. (4.3) requires the calculation of the operation of $\Phi_n(-i\hat{\mathbf{H}}_{\text{norm}})$ on $\psi(0)$. This is accompanied by the recursion relation of the Chebyshev polynomials

$$\phi_{n+1} = -2i\hat{\mathbf{H}}_{\text{norm}}\phi_n + \phi_{n-1} \tag{4.5}$$

and $\phi_n = \Phi_n(-i\hat{\mathbf{H}}_{\text{norm}})\,\psi(0)$. The recurrence is started by $\phi_0 = \psi(0)$ and $\phi_1 = -i\hat{\mathbf{H}}_{\text{norm}}\psi(0)$. In order to save storage, only the vectors which are the result of the nth and $(n-1)$th operations are saved. The result is accumulated in ψ. The number of expansion terms needed to converge the sum in (4.1) is determined by the size of the time-energy phase space volume: $\alpha = \Delta E_{\text{grid}} \cdot t/2\hbar$. Examining the expansion coefficients as a function of n, one finds that when n becomes larger than α, the Bessel functions $J_n(\alpha)$ decay exponentially. This means that in a practical implementation, the maximum order N can be chosen such that the accuracy is dominated by the accuracy of the computer. The total number of expansion terms will be slightly larger than the theoretical limit $\Delta E_{\text{grid}}\,t/2\hbar$. One of the most important aspects of the Chebyshev propagation scheme is that the error is uniformly distributed over the entire range of eigenvalues (which can be a corresponding disadvantage if the eigenvalues are *not* uniformly distributed). The method is not unitary but because of its extreme accuracy the deviation from unitarity can be used as an accuracy check. For this reason the Chebyshev scheme was chosen as a benchmark for the other propagation schemes with a uniform error set to be less than 10^{-14}.

One drawback of a global evolution method is that intermediate results, which may carry much information, are not obtained. One way to overcome this problem is to split the propagation into smaller intervals. The practical lower limit of the Chebyshev expansion is approximately 10 terms. The reason is that the extra terms above $n = \alpha$ which are needed to converge the sum begin to dominate, making

the approximation inefficient. For example, a 10-term expansion with specified accuracy of 10^{-5} has an efficiency, α/N, of 20%. For interpretation of intermediate results, this time interval is usually enough, but many applications require the calculation of correlation functions at very short intervals. The problem can be overcome by considering that only the expansion coefficients in (4.3) are time dependent. The Chebyshev polynomial operations, $\phi_n = \Phi_n(-i\hat{\mathbf{H}}_{\text{norm}})\psi(0)$ which require most of the calculation effort, are time independent. This means that the expansion coefficients a_n can be recalculated for many intermediate times. For example, when the correlation function $\langle\xi(0)|\,\hat{\mathbf{O}}\,|\psi(t')\rangle$ is desired at an intermediate time t', it can be approximated by

$$\langle\xi(0)|\,\hat{\mathbf{O}}\,|\psi(t')\rangle \approx \sum_{n=0}^{N} a_n\left(\frac{\Delta E_{\text{grid}}\, t'}{2\hbar}\right)\langle\xi(0)|\,\hat{\mathbf{O}}\,|\phi_n\rangle. \tag{4.6}$$

Note that the accumulator which is the left-hand side of Eq. (4.6) is a scalar and therefore the storage requirements of the calculation are only slightly increased. It should be noticed that the Chebyshev scheme becomes unstable if the energy range ΔE is underestimated.

The Chebyshev scheme can be used to propagate ψ in imaginary time [12]. This method can be useful in obtaining the ground state or thermal states. In order to change the propagation scheme an analytic continuation is performed, the expansion coefficients in Eq. (4.4) are modified to $2I_n(\alpha)$, and the recursion relation (4.5) is changed to

$$\phi_{n+1} = 2\hat{\mathbf{H}}_{\text{norm}}\phi_n - \phi_{n-1}. \tag{4.7}$$

To conclude, the global Chebyshev polynomial approximation is an extremely accurate scheme with very high efficiency in relation to the maximum frequency determining the grid ω_{grid}, $\eta_{Dg} = 2$ when $\Delta t \to \infty$. The method does not conserve norm or energy which can be used to estimate the error. Time reversal symmetry is built into the expansion coefficients. The method can work with any functional form of Hamiltonian operator provided an estimate of the eigenvalue range can be made. If this range is underestimated the method becomes unstable. The method is not recommended for time dependent problems and for wavefunctions which occupy a very small spectral range in relation to the spectral range of the grid for which the efficiency is small, $\eta_g \ll 1$.

V. The Second-Order Differencing Scheme (SOD)

The simplest scheme for propagating equation (1.1) is to expand the evolution operator

$$\hat{\mathbf{U}} = \exp(-i\hat{\mathbf{H}}\,\Delta t/\hbar) \tag{5.1}$$

in a Taylor series

$$\exp(-i\hat{\mathbf{H}}\,\Delta t/\hbar) = 1 - i\hat{\mathbf{H}}\,\Delta t/\hbar + \cdots . \tag{5.2}$$

It has been found that a numerical algorithm based on this expansion is not stable [2]. The instability comes about because the scheme does not conserve the time reversal symmetry of the Schrödinger equation. With a symmetric modification of the expansion, stability is obtained. One way to formulate the scheme is to use second-order differencing (SOD) to approximate the time derivative in Eq. (1.1). Another formulation uses the symmetric relation

$$\psi(t+\Delta t) - \psi(t-\Delta t) = (e^{-i\hat{\mathbf{H}}\Delta t/\hbar} - e^{i\hat{\mathbf{H}}\Delta t/\hbar})\,\psi(t) \tag{5.3}$$

and then by expanding $\hat{\mathbf{U}} = \exp(-i\hat{\mathbf{H}}\,\Delta t/\hbar)$ and $\hat{\mathbf{U}}^*$ in a Taylor series, the explicit second-order propagation scheme is obtained

$$\psi(t+\Delta t) \approx \psi(t-\Delta t) - 2i\,\Delta t\,\hat{\mathbf{H}}\psi(t)/\hbar. \tag{5.4}$$

If the Hamiltonian operation is Hermitian, the SOD propagation scheme preserves norm and energy. A good way to investigate this is to write the propagation as a discrete mapping

$$\begin{pmatrix} \psi^{n+1} \\ \psi^{n} \end{pmatrix} = \begin{bmatrix} 1 - 4\Delta t^2\,\hat{\mathbf{H}}^2/\hbar^2 & -2i\,\Delta t\,\hat{\mathbf{H}}/\hbar \\ -2i\,\Delta t\,\hat{\mathbf{H}}/\hbar & 1 \end{bmatrix} \begin{pmatrix} \psi^{n-1} \\ \psi^{n-2} \end{pmatrix}, \tag{5.5}$$

where n is the index of the time step. The eigenvalues of this propagation matrix are

$$\lambda_{1,2} = 1 - 2\Delta t^2\,\hat{\mathbf{H}}/\hbar^2 \pm \frac{2\Delta t\,\hat{\mathbf{H}}}{\hbar}\left(\frac{\Delta t^2\,\hat{\mathbf{H}}^2}{\hbar^2} - 1\right)^{1/2}. \tag{5.6}$$

The discrete map is area preserving if the determinant of the propagation matrix is unity which is equivalent to $\lambda_1\lambda_2 = 1$. This implies norm conservation in the adjoint space [6]. The mapping is stable only if the eigenvalues $\lambda_{1,2}$ are complex. Real eigenvalues lead to exponential growth as λ_1^n because $\lambda_1 > 1$. This condition supplies the stability criterion of the discrete map

$$\frac{\Delta t^2\,\hat{\mathbf{H}}^2}{\hbar^2} - 1 < 0 \tag{5.7}$$

which has to be true for all eigenfunctions of the Hamiltonian operator leading to

$$\Delta t < \frac{\hbar}{E_{\max}}, \tag{5.8}$$

where $E_{\max}$ is the eigenvalue with largest absolute value of the discrete Hamiltonian

operator. If the time step exceeds the stability limit, exponential solutions take over, resulting in a numerical overflow. This fact can be used to obtain empirically the stability limit [6].

The norm and energy conservation of the SOD scheme in the adjoint space is a consequence of the time reversal symmetry of the scheme and of the Hermitian property of the Hamiltonian operator. This can be seen by multiplying Eq. (5.4) by $\psi^*(t)$ and multiplying the conjugate equation by $\psi(t)$, adding the two equations, and summing over all space which leads to

$$\langle \psi(t-\Delta t) | \psi(t) \rangle = \langle \psi(t) | \psi(t+\Delta t) \rangle = \text{const.} \tag{5.9}$$

The energy conservation is obtained in a similar way by multiplying Eq. (5.4) by $(\hat{\mathbf{H}}\psi)^*$. The result is

$$\langle \psi(t-\Delta t) | \hat{\mathbf{H}} | \psi(t) \rangle = \text{const.} \tag{5.10}$$

It should be noted that in a consistent scheme matrix elements should also be calculated at successive times for example $\langle \hat{\mathbf{V}}(t) \rangle = \langle \psi(t-\Delta t) | \hat{\mathbf{V}} | \psi(t) \rangle$. Also, the exact form of norm and energy conservation, for example, $\langle \psi(t), \psi(t) \rangle$, can be monitored as a check of the calculated error, since neither of these values is rigorously conserved by the differencing scheme.

Because of this particular form of norm and energy conservation, the error in propagation accumulates in the phase. In order to obtain an estimate of this error, consider the propagation of an eigenfunction ϕ_m with eigenvalue E_m. The eigenvalues of the propagation matrix become

$$\lambda_{1,2} = 1 - \frac{2\Delta t^2 E_m^2}{\hbar^2} \pm \frac{2\Delta t E_m}{\hbar} \left(\frac{\Delta t^2 E_m^2}{\hbar^2} - 1 \right)^{1/2}. \tag{5.11}$$

By comparing Eq. (5.11) with the eigenvalue of the exact propagation operator,

$$\lambda_{\text{exact}} = e^{-2iE_m \Delta t/\hbar},$$

one finds that the error in propagation by the SOD method per time step is

$$\text{error} \approx \frac{(\Delta t E_m)^3}{3\hbar^3}. \tag{5.12}$$

Propagating N times accumulates this error N times. First, it should be noticed that the error is not uniform and is large for large eigenvalues of ψ. To minimize the error in phase, it is customary to choose a time step, Δt, five times smaller than the stability limit, $\Delta t < \hbar/(5\Delta E_{\text{grid}})$. The resulting error for N steps becomes error $\approx N/375$ which allows a few hundred propagation steps before errors in interference terms become important. One should notice that by shifting the energy, and by adding a constant to the Hamiltonian, one can predetermine the region in energy with minimum error. Considering the scaling of the numerical effort for a

fixed time, the error scales as $O(1/N^2)$, where N is the number of times the Hamiltonian operator is called. For a constant error the numerical effort scales as $O(t^{3/2})$.

Another important consideration is that the SOD scheme is only stable if the Hamiltonian operator is strictly Hermitian. This means it cannot be used for propagating in imaginary time and that, if an optical potential is used for absorbing boundary conditions, a first-order scheme should be used to propagate this part.

Initializing the SOD

The SOD scheme requires two initial conditions, in order to start the propagation. The initialization scheme should have at least the same accuracy as the rest of the propagation. A common method is to start by a first-order scheme for half a time step, then use the SOD scheme to propagate another half step, such that the two initial conditions $\psi(t)$ and $\psi(t+\Delta t)$ are obtained. A more symmetric scheme in relation to time reversal is to propagate half a step backward and obtain $\psi(t-\Delta t)$ and then half a step forward and obtain $\psi(t+\Delta t)$. The propagation then continues as usual. Intermediate results are obtained by the approximation

$$\psi(t) \approx 1/2\{(\psi(t-\Delta t/2)+\psi(t+\Delta t/2) + \frac{i}{\hbar}\Delta t/2(\hat{\mathbf{H}}\psi(t+\Delta t/2)-\hat{\mathbf{H}}\psi(t-\Delta t/2))\} \tag{5.13}$$

which is accurate up to second order.

The method is unitary and conserves norm and energy. The method is conditionally stable if $\Delta t < \hbar/\Delta t < \hbar/E_{\max}$ and $V_{\min} > 0$. This means that the spatial representation should be well balanced with the time propagation $\omega_w/\omega_g = \eta_g \approx 1$ otherwise unnecessarily short time steps result. Time reversal symmetry is built into the scheme.

VI. Split Operator Method (SPO)

The split operator method takes advantage of the ease of treating operators in their diagonal representations. Its first application [5] was to the paraxial wave equation of optics which is mathematically identical to the Schrödinger equation. The short time propagator, $\hat{\mathbf{U}}(\Delta t)$ can be approximated by [4]

$$\hat{\mathbf{U}}(\Delta t) = \exp\left(-\frac{i}{\hbar}\hat{\mathbf{H}}\,\Delta t\right) \approx \exp\left(-\frac{i}{2\hbar}\hat{\mathbf{K}}\,\Delta t\right) \times \exp\left(-\frac{i}{\hbar}\hat{\mathbf{V}}\,\Delta t\right)\exp\left(-\frac{i}{2\hbar}\hat{\mathbf{K}}\,\Delta t\right) + O(\Delta t^3). \tag{6.1}$$

Here the kinetic energy operator $\hat{\mathbf{K}} = \hat{\mathbf{P}}^2/2m$ is diagonal in momentum space, while the potential energy $\hat{\mathbf{V}}$ is diagonal in configuration space. The truncation

error is determined by the next higher commutator between the potential and the kinetic energy and will vary with the value of these terms. For typical potential function choices, this error will be controlled by the fourth derivative of the potential function and the cube of the time increment. The error enters in the exponent of the propagator and is often smaller in applications than simple upper bound

points. Thus, the kinetic energy part of $\hat{\mathbf{U}}$ can be evaluated by

$$\exp\left(-\frac{i}{2\hbar}\hat{\mathbf{K}}\,\Delta t\right)=\mathbf{Z}\exp\left(-\frac{i}{2\hbar\,\mathbf{T}\,\Delta t}\right)\mathbf{Z}^{\dagger}, \tag{6.2}$$

where $Z^{\dagger}$ is a finite Fourier transform with matrix elements of the form $Z_{ij}^{\dagger}=N^{-1/2}\exp(i\mathbf{k}_i\cdot\mathbf{r}_i)$ and $\mathbf{T}$ is the diagonal kinetic energy with elements of the form $\hbar^2k^2/2m$. The symmetrized form of $\hat{\mathbf{U}}$ above is useful for formal discussion; in practice, the kinetic energy terms can be merged so that one alternates between full time steps of free propagation and potential updating. The method is practical even when many plane waves are required, since the fast Fourier transform algorithm requires only $O(N\log N)$ multiplications, allowing two or three spatial dimensions to be handled.

The grid representation is accurate provided the wavefunction is band-limited and of finite support—that is, of finite extent in both configuration and momentum space. For a time-independent Hamiltonian function, maximum speed is achieved by storing the $2N$ exponential factors of form $\exp(-(i/\hbar)\hat{\mathbf{V}}\,\Delta t)$ and $\exp(-(i/\hbar)\hat{\mathbf{T}}\,\Delta t)$ at the start. A typical computational step then consists of N multiplications by the potential energy factors, a Fourier transform, N multiplications by kinetic energy factors, and finally, an inverse Fourier transform.

This method is unconditionally stable and norm preserving. The former property allows one to choose the time step according to the energy range of interest, not necessarily that given by the maximum allowable kinetic energy $(\hbar\pi/\Delta x)^2/2m$. This is particularly true when the bound states are of primary interest and their energies are determined from an auto-correlation function. In this case, high energy continuum states are out of phase, but this causes no problem with finding the bound state energies. The time step is determined by the binding energy.

This form of the short time propagator is similar to a quantum mechanical "kicked rotor"—alternating free propagation with periodic impulses due to the potential. It can also be thought of as a Feynman path integral. That is, Eq. (6.1) is a second-order approximation to the Trotter product form for the full propagator [13]

$$e^{i(\mathbf{A}+\mathbf{B})t}=\lim_{n\to\infty}(e^{i\mathbf{A}t/n}e^{i\mathbf{B}t/n})^n \tag{6.3}$$

which displays the connection to the Feynman path integral explicitly. Furthermore, the algorithm extends naturally to higher even power symmetric expansions

[14]. It is uncertain whether the gain in accuracy is offset by the numerical effort required. The calculations carried out in Ref. [14] used a low order finite difference scheme for the kinetic energy and this error might dominate the results. The algorithm cannot handle operators that mix spatial coordinates and momenta. The method has been used to treat bound eigenstate determination and wavepacket scattering [4]. Time dependent Hamiltonian functions can be treated if the time step is chosen small compared to a characteristic time. The scheme does not conserve energy and is limited to Hamiltonian operators which can be split into two non-commuting parts with a simple transformation between them. The method is recommended for $\eta_g \ll 1$. The method has been extended also for propagations in imaginary time.

VII. Short Iterative Lanczos Propagation (SIL)

The Lanczos algorithm has been developed and applied in several disciplines [15]. It was originally proposed as a reduction technique for linear operators, producing matrices in Hessenberg form [16]. As such, it is known to be unstable for large orders. On the other hand, its use as a *low order* scheme for producing a convenient tridiagonal operator form should not be underestimated. In particular, the algorithm should be useful as a time propagation scheme for the non-relativistic Schrödinger equation. This approach has indeed been pursued for time independent Hamiltonian functions using basis set expansion techniques [17] and for large time step correlation functions [15]. This method should also be effective, in principle, for grid methods which could encompass either time dependent or time independent Hamiltonian operators. The time independent applications have been investigated by Park and Light [18] which motivated the present work. Indeed, the time dependent methods reflect a different choice of "basis" set expansion—that is, the use of a discrete, local representation; otherwise the grid methods are completely analogous to the previous time independent studies. Since it is a short-time propagation scheme, the procedure might offer significant advantages in flexibility and efficiency: there would be no restriction on the form of the operator; low order expansions might be sufficiently accurate; and variable time steps or variable order with error control are possible during time propagation.

Background

The iterative Lanczos reduction scheme entails the construction of a three-term recurrence relation within the Krylov subspace generated by the linear operator. The Krylov subspace is defined by the action of a linear operator on an initial vector $\psi(0)$; thus the Krylov subspace of order $(N-1)$ generated from a Hamiltonian operator is

$$u_j = \hat{\mathbf{H}}^j \psi(0), \tag{7.1}$$

where the set of vectors u_j spans a projected or reduced subspace of the original

infinite dimensional space. Note that this cyclic subspace is, in general, a complex vector subspace. The Lanczos recurrence generates a set of orthogonal polynomials lying within the subspace which represents a finite polynomial approximation to the operator. If the linear operator is itself finite dimensional, then the method is exact, since every N-dimensional linear operator satisfies its Nth-order characteristic polynomial equation (Cayley–Hamilton theorem). The algorithm thus has the very attractive feature of reducing to an exact technique for finite dimensions which in turn suggests that a suitably projected infinite dimensional space might be accurately approximated therein.

An unusual feature of this algorithm is its dependence on both the linear operator *and* upon the initial approximating vector. That is, the polynomial set generated will depend upon the initial vector chosen to generate the Krylov subspace. In the specific case of the non-relativistic Schrödinger equation, the unitary evolution propagator, $\hat{\mathbf{U}}(t)$, expressed as in Eq. (4.1),

$$\hat{\mathbf{U}}(t) = e^{-(i/\hbar)\hat{\mathbf{H}}t} \approx \sum_{n=1}^{N} a_n P_n(-(i/\hbar)\,\hat{\mathbf{H}}t). \tag{7.2}$$

This expression clearly depends upon the order of the polynomial approximation (the choice of N), the linear operator $\hat{\mathbf{H}}$, and, for the Lanczos scheme, the initial vector chosen will influence the expansion coefficients a_n. This is in contrast to the Chebyshev approach, for example, where the coefficients a_n are known, fixed quantities (integral order Bessel functions) which are generated initially for all time. Furthermore, the order of the expansion (number of Bessel functions used) depends only on the energy range and time step chosen. The Lanczos method, on the other hand, tailors the approximating polynomial set to both the operator and initial vector. Since this is an orthogonal set, Gaussian quadrature accuracy of order $2n-1$ is expected for n points.

The Lanczos tridiagonal construction is initialized by

$$q_0 = \psi(0)$$

and

$$\hat{\mathbf{H}}_{q_0} = \alpha_0 q_0 + \beta_0 q_1 \tag{7.3a}$$

and given generally by

$$\hat{\mathbf{H}}_{q_j} = \beta_{j-1} q_{j-1} + \alpha_j q_j + \beta_j q_{j+1}, \tag{7.3b}$$

where the coefficients are

$$\alpha_j = (q_j, \hat{\mathbf{H}}_{q_j}) \tag{7.4a}$$

and

$$\beta_{j-1} = (q_{j\ \ 1}, \hat{\mathbf{H}}_{q_j}). \tag{7.4b}$$

The inner product implied by this notation is the usual complex Hilbert space inner product. The projected subspace representation of the Hamiltonian operator has the tridiagonal form

$$\hat{\mathbf{H}}_N = \begin{pmatrix} \alpha_0 & \beta_0 & 0 & \cdots & \cdots & \cdots & 0 \\ \beta_0 & \alpha_1 & \beta_1 & 0 & \cdots & \cdots & 0 \\ 0 & \beta_1 & \alpha_2 & \beta_2 & 0 & \cdots & 0 \\ \vdots & \vdots & \ddots & \ddots & \vdots & \vdots & 0 \\ 0 & \cdots & \cdots & \cdots & \beta_{N-3} & \alpha_{N-2} & \beta_{N-2} \\ 0 & \cdots & \cdots & \cdots & \cdots & \beta_{N-2} & \alpha_{N-1} \end{pmatrix}. \tag{7.5}$$

The approximate unitary propagation operator becomes

$$\hat{\mathbf{U}}(\Delta t) \approx \hat{\mathbf{U}}_N(\Delta t) = e^{-(i/\hbar)H_N \Delta t} \tag{7.6}$$

and

$$\psi(\Delta t) \approx \hat{\mathbf{U}}_N(\Delta t)\, \psi(0). \tag{7.7}$$

The propagation of the initial wavefunction is now described in the projected subspace by a tridiagonal Hamiltonian operator. Diagonalization of this operator can be efficiently performed so that practical evaluation of the propagation is given by

$$\hat{\mathbf{U}}(\Delta t) = Z^{\dagger} e^{-(i/\hbar)D_N \Delta t} Z, \tag{7.8}$$

where the unitary matrix Z diagonalizes $\hat{\mathbf{H}}_N$ ($Z^{\dagger}$ is the Hermitian transpose of Z), and D_N is the diagonal matrix of eigenvalues. For emphasis, the propagated wavefunction becomes

$$\psi(\Delta t) = \hat{\mathbf{U}}_N(\Delta t)\, q_0. \tag{7.9}$$

Error estimates follow from the magnitude of the first vector, $q_N(\Delta t)$, lying outside of the Krylov space. This magnitude, $|q_N(\Delta t)|$, could then be used as a tolerance parameter in a variable time step or variable order determination. The calculated error can be approximately evaluated, following Park and Light [18], as the product of the off-diagonal elements

$$q_N(\Delta t) \approx \frac{(-i\,\Delta t)^{N-1}}{(N-1)!} \prod_{k=0}^{N-1} \beta_k, \tag{7.10}$$

or more directly by explicit calculation during the evaluation of the wavevector components. Another source of error is produced from the orthogonalization procedure in Eq. (7.3). It is for this reason that the method is restricted to short time steps and relatively low order.

To conclude, the method is unitary and conserves norm and energy. The scheme is unconditionally stable and therefore can be used for unbalanced spectral range when $\eta_g \ll 1$.

VIII. Numerical Results

The purpose of this section is to gain insight into the numerical behavior of the propagation schemes using a physical example [19]. A one-dimensional Morse potential with the mass and potential parameters describing the ground electronic and vibrational state of H_2 was chosen. A grid of 256 points with $\Delta x = 0.1$ was used for the spatial representation. A time step of $\Delta t = 12.0$ was selected for the generation of the reference ("exact") wavefunction. Table I summarizes the potential grid and propagation parameters used. These parameters define a grid frequency of $\omega_g = 1.016$. The calculations were carried out for two initial states. In the first mode a scattering event was simulated by positioning the initial wavefunction in the [illegible] used which allowed ω_w to vary by changing the width of the wavefunction. For a width of 2 a.u. and a tolerance of 10^{-5}, the wavefunction frequency ω_w is 0.05. The second mode simulated a completely bound wavefunction (not an eigenfunction) which oscillates in the bound part of the potential.

The first set of runs was chosen to study the accumulated error in each method. Figure 1 displays this error as a function of time. The SOD results for the scattering initial state are given in Fig. 1a. A linear dependence of the accumulated error is found which is expected for a stepwise integrator. The graph also shows the convergence of the method as the time step decreases. Similar error relationships hold for the bound initial state choice. The same behavior is observed in the overlap phase error which is defined as the phase of the overlap between the reference wavefunction and the approximate one $(\psi_{CH}(t), \psi_{approx}(t))$. Figure 1b shows the scaling relation of the accumulated overlap error with respect to time for the SPO technique. The convergence properties of the method are very different from the SOD scheme: the large time step calculations have an oscillatory behavior in time. This behavior is a consequence of the non-uniform behavior of the commutation

TABLE I

Potential, grid, and Propagation Parameters Used
(Atomic Units Throughout)

		Scattering	Bound
$\alpha = 1.0144$ bohr^{-1}	$\Delta t = 12.0$	$x0 = 14.0$	$x0 = 5.0$
$D = 0.1744$ hartree	$\Delta x = 0.10$	$p0 = -10.0$	$p0 = -1.0$
$r_e = 1.40$ bohr	$N_{grid} = 256$	0.25	$\sigma = 1.0$
	$N_{times} = 7000$		

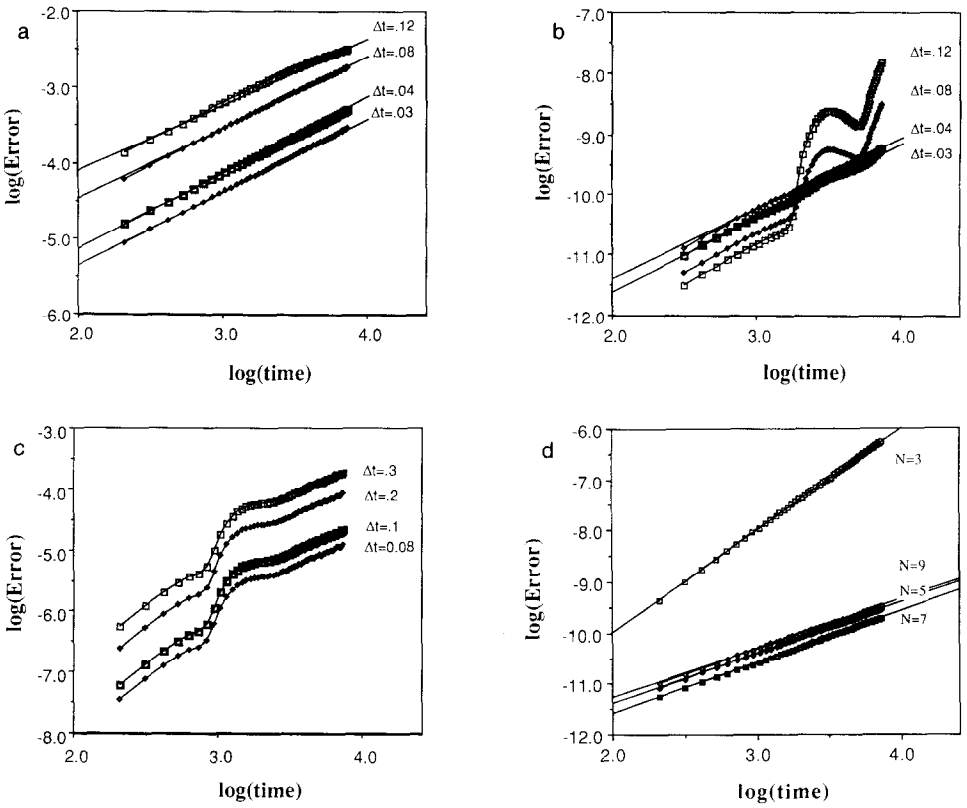

FIG. 1. (a) SOD initial scattering state. Logarithm, base 10, of the accumulated overlap amplitude error as a function of logarithmic time for the SOD propagation method. The overlap error is defined to be $1-|(\psi_{CH}(t), \psi_{SOD}(t))|$; the four plots display different choices of time step: $\Delta t = 0.12$, 0.08, 0.04, and 0.03. The Chebyshev wavefunction with a uniform error of 10^{-14} was used as the reference. The initial conditions correspond to a scattering event. (b) SPO bound initial state. Logarithm of the accumulated amplitude error as a function of logarithmic time for the split operator propagation method. The error calculations are the same as Fig. 1a. The initial condition corresponds to a bound state. (c) SPO scattering initial state. Same as Fig. 1b for the overlap phase error for a scattering initial state for the split operator propagator. The phase error is defined to be the phase of the overlap $(\psi_{CH}(t), \psi_{SPO}(t))$. (d) SIL bound initial state. The overlap phase error as a function of logarithmic time for a bound initial state for the SIL propagation. The four plots display different orders (3, 5, 7, and 9) of interpolating polynomial over the fixed time step.

relations as a function of the average position of the wavefunction. Recall that the source of error in the SPO is the neglect of high order commutators. The converged results do possess a linear accumulation of error with time. Figure 1c displays the overlap phase error for the scattering state calculation. Strongly nonlinear dependence is observed for all time step sizes. The SIL propagation results are given in Fig. 1d for a bound state evaluation with different powers of interpolating polynomial. The third order polynomial has a quadratic overlap amplitude error

accumulation while the higher order polynomials have the expected linear dependence. The error saturates rapidly using higher orders. Similar results were seen for the higher order polynomials in the phase error but the third-order polynomial showed cubic error accumulation which indicates that the phase error grows more rapidly than the amplitude error. For comparison purposes, it should be noted that the Chebyshev scheme has a constant error scaling with respect to time.

The next series of computations evaluated the scaling of the error for fixed total propagation time. Figure 2a displays this relation for the SOD. Note the overall

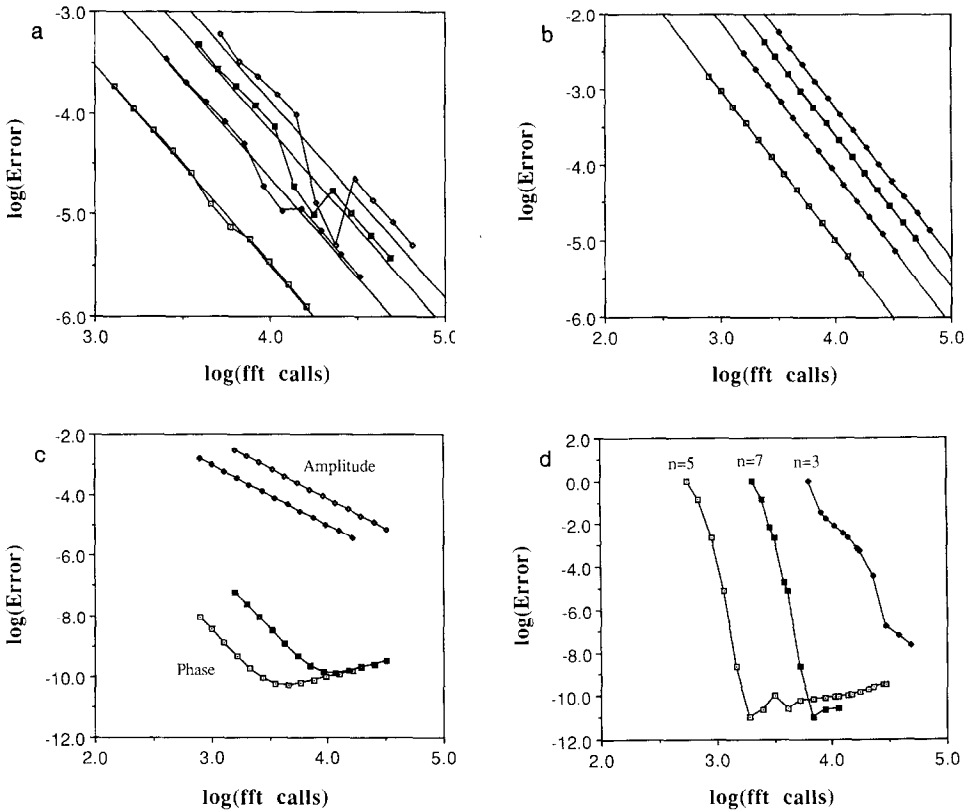

FIG. 2. (a) SOD bound initial state. The logarithm of the amplitude error as a function of the logarithm of the numerical effort for the SOD propagation. The numerical effort is measured by the number of FFT calls, at a fixed time. Results for four times—600, 1200, 1800, and 2400 atomic units—are shown for the bound initial state with the earliest time in the leftmost plot. The linear fits have an approximate slope of -2, and the fixed error accumulates in time as $t^{3/2}$. (b) SPO bound initial state. Same as Fig. 2a for the split operator propagator phase error. The linear fits have a slope of -2 which is expected from a second-order method. (c) SPO bound initial state. A comparison between phase and amplitude error for the SPO propagator for two times: 600 and 2400 atomic time units. The lower plots correspond to the amplitude error; the upper plots correspond to the phase error. (d) SIL bound initial state. Same as Fig. 2a for the SIL propagator amplitude error. Results for three polynomial orders—3, 5, and 7—are shown for 2400 atomic time units.

cubic dependence of the error upon numerical effort which holds for both initial states and for both phase and amplitude errors. There is an exceptional case for intermediate runs where the error decreases in amplitude, as shown in Fig. 2a, but increases for the phase (not plotted). Figures 2b contains the same information for the split operator phase error. Notice the quadratic convergence of the error with respect to numerical effort, as expected for a second-order method. Figure 2c compares the amplitude and the phase error of the split operator method. There are several orders of magnitude difference in these two errors. Figure 2d shows the convergence of the different orders of the SIL propagation scheme. No simple linear relation fits the data which implies faster than power law convergence. Eventually, the error saturates with numerical effort indicating that the roundoff errors in the SIL procedure begin to accumulate.

Finally, the sensitivity of initial state choice for the Lanczos method was investigated for the same initial conditions for scattering with a variation in the width of the initial wavepacket. Figures 3a and b display the variance of initial condition choice for the scattering initial conditions using the split-operator and the SIL algorithms. In these plots, the width of the wavefunction (the parameter σ) was varied from 0.15 to 0.30, which corresponds to a variance in energy of 1.24×10^{-4} to 4.94×10^{-4}. The error in the overlap amplitude clearly indicates the sensitivity of these algorithms to the spectral range of the initial choice. There is a pronounced difference in the phase error between the two methods, much less so for the amplitude error. The Lanczos phase error is very sensitive to the choice of initial state, whereas the split operator has no analogous sensitivity. Both methods show similar behavior for the amplitude error. Note also that the error scaling with time is constant for the narrow widths while a linear dependence holds for the broader widths.

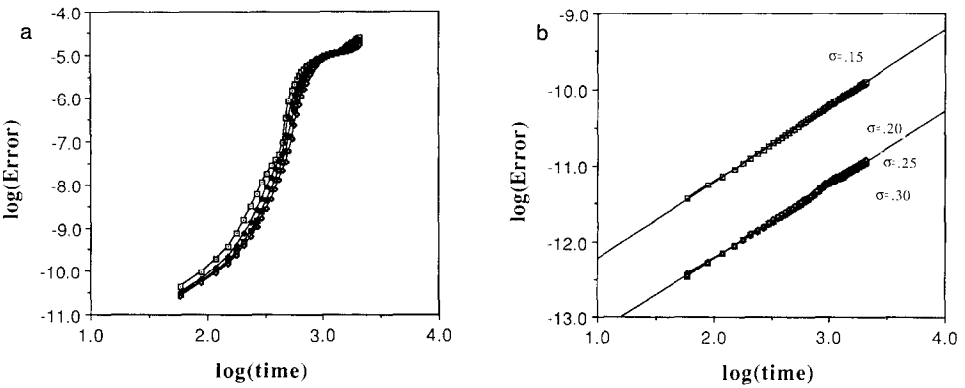

FIG. 3. (a) Phase error dependence of the SPO propagator as a function of time for different choices of the initial scattering state wavefunction. Four choices of width (parameter σ) were made: 0.15, 0.20, 0.25, and 0.30. The time step was 0.04 atomic units. (b) Same as Fig. 3a for the SIL propagator. A fifth-order interpolating polynomial was used.

IX. Discussion

A few general conclusions about the error scaling relationships for the different methods can be drawn from the simple case studied above. These conclusions corroborate numerically the brief theoretical analysis given previously. The methods are briefly compared in Table II. From Fig. 1a, it is apparent that the SOD error accumulates linearly with the number of steps with the error per step scaling as $(\Delta t)^3$ (Eq. (5.12)); the accumulated error scales as the inverse square of the number of time steps as demonstrated in Fig. 2a. Also, the error in the phase and amplitude have similar behavior and are approximately equal.

The split operator technique possesses the same quadratic dependence in the error as the SOD, since they are both second-order methods (Fig. 2b). On the other hand, there is a remarkable discrepancy in the amplitude and phase errors: they differ by approximately five orders of magnitude. This observation indicates that discretion must be used when accuracy is required for the phase of the wavefunction. For example, in time dependent problems, the method should be used as a second-order method for consistency; the half-step must be calculated whenever the potential is updated otherwise the algorithm becomes a first-order scheme.

The most striking feature of the SIL is the rapid convergence of the algorithm as a function of interpolating order and time step. The error made in the phase and amplitude are approximately equal and have the same trend. The error saturates faster than power law dependence. Sensitivity of the method to the spectral range of the initial wavefunction choice was observed (Fig. 3b). Finally, the CH method is unique in the sense that it has no accumulated error. The amplitude and phase error are approximately equal.

The phase error as a function of time calculated by each of the techniques is plot

method. The relative ordering of the accuracy of each of the methods is obvious. A striking demonstration of the scaling of the error with numerical effort is shown for the four methods in Fig. 5. The exponential convergence of the CH method is

TABLE II

Comparison of the Algorithms

Method	SPO	SOD	Chebyshev	Lanczos
Norm	Unitary	Unitary	Not unitary	Unitary
Energy	Not conserved	Conserved	Not conserved	Conserved
Stability	Stable	Unstable	Unstable	Stable
Error type	Commutator Accuracy	$(E_m/\Delta t)^3$	Arbitrary accuracy	Arbitrary accuracy
Error scaling	Quadratic	Quadratic	Exponential	High order
Hamiltonian	No mixed terms $(f(x)\,g(p))$	No restriction	Time independent	No restriction
Storage arrays	2	3	4	Order + 1

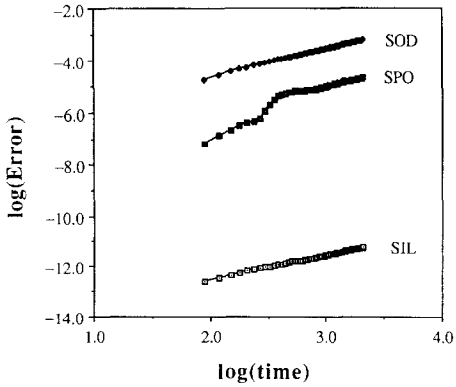

FIG. 4. A comparison of the phase error as a function of time for three propagators with bound initial state conditions.

clearly superior to all other methods for this calculation. The second best choice would be the SIL, with its fast convergence with numerical effort. The SPO is definitely superior to the SOD by about a factor of ten which has been noted empirically by several researchers. For a different choice of phase or increase in the spectral range, the CH results would be shifted to the right in Fig. 5, while the SIL and SPO are intensive to this change. The implication is that for problems with extremely large spectral range, the SIL will become more efficient than the CH scheme.

The three older methods (SOD, SPO, and CH) have been successfully applied to multi-dimensional problems and non-Cartesian coordinate choices. Parenthetically, after the initiation of this research, another interpolating polynomial method has been developed which has similar properties to the SIL [20]. Also it could be mentioned that methods based upon the Krylov subspace scheme can be extended to

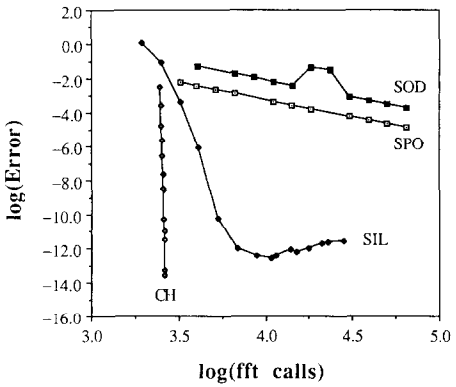

FIG. 5. Phase error as a function of numerical effort for the four methods at a fixed time of 2400 atomic units. The bound initial conditions are used and the numerical effort is measured by the number of FFT calls.

variable time step algorithms which can offer a significant advantage for explicitly time dependent operators.

In conclusion, each method has its merits and demerits. For convenience, Table II lists some of the more important features in the comparison of the different algorithms. Specific problems will of course have different requirements for the appropriate propagator choice and, as always, the potential user must use discretion in making this choice. The overall conclusion appears that for generality, flexibility, and accuracy the Chebyshev method should be the method of choice for explictly time independent Hamiltonian operators. For explictly time dependent operators or problems with large spectral range, the Lanczos algorithm offers great accuracy and efficiency for a broad class of potentials.

ACKNOWLEDGMENTS

This work was performed in part under the auspices of the U.S. Deptartment of Energy by Lawrence Livermore National Laboratory under Contract W-7405-ENG-48. The authors wish to thank the CECAM director, Dr. C. Moser, for his hospitality, and especially for the provision of financial and computational resources for the workshop.

REFERENCES

1. E. A. McCullough, Jr., and R. E. Wyatt, *J. Chem. Phys.* **51**, 1253 (1969); **54**, 3592 (1971).
2. A. Askar and A. S. Cakmak, *J. Chem. Phys.* **68**, 2794 (1978).
3. C. Leforestier, *Chem. Phys.* **87**, 241 (1984).
4. M. D. Feit, J. A. Fleck, Jr., and A. Steiger, *J. Comput. Phys.* **47**, 412 (1982).
5. M. D. Feit and J. A. Fleck, Jr., *Appl. Opt.* **17**, 3990 (1978); **18**, 2843 (1979); **19**, 1154, **19**, 2240, 3140 (1980).
6. D. Kosloff and R. Kosloff, *J. Comput. Phys.* **52**, 35 (1983); R. Kosloff and D. Kosloff, *J. Chem. Phys.* **79**, 1823 (1983).
7. D. Kosloff and E. Baysal, *Geophysics* **47**, 1402 (1982).
8. R. Kosloff, *J. Phys. Chem.* **92**, 2087 (1988).
9. J. W. Cooley and J. W. Tukey, *Math. Comput.* **19**, 297 (1965); C. Temperton, *J. Comput. Phys.* **52**, 1 (1983).
10. E. Tadmor, *SIAM J. Numer. Anal.* **23**, 1 (1986); D. Gottlieb and S. A. Orszag, *Numerical Analysis of Spectral Methods: Theory and Applications* (SIAM, Philadelphia, 1977).
11. H. Tal-Ezer and R. Kosloff, *J. Chem. Phys.* **81**, 3967 (1984).
12. K. T. R. Davies, H. Flocard, S. Kreiger, and M. S. Weiss, *Nucl. Phys. A* **342**, 111 (1980); R. Kosloff and H. Tal-Ezer, *Chem. Phys. Lett.* **127**, 223 (1986).
13. L. S. Schulman, *Techniques and Applications of Path Integration* (Wiley-Interscience, New York, 1981).
14. H. De Raedt, *Comput. Phys. Rep.* **7**, 1 (1987).
15. C. J. Lanczos, *J. Res Natl. Bur. Stand.* **45** 255 (1950); R. Haydock, *J. Phys. C* **14**, 229 (1981).
16. J. H. Wilkinson, *The Algebraic Eigenvalue Problem* (Oxford Univ. Press, London, 1965).
17. G. Moro and J. H. Freed, *J. Chem. Phys.* **74**, 3757 (1981); H. Köppel, W. Domcke, and L. S. Cederbaum, *Adv. Chem. Phys.* **57**, 59 (1984); A. Nauts and R. E. Wyatt, *Phys. Rev. Lett.* **51**, 2238 (1983).
18. T. J. Park and J. C. Light, *J. Chem. Phys.* **85**, 5870 (1986).
19. A CRAY-compatible version of the comparison code used is available from one of the authors (C. Cerjan).
20. H. Tal-Ezer, R. Kosloff, and C. Cerjan, *J. Comput. Phys.*, submitted.